Dynamics of Reaction-Diffusion Oscillators in Star and other Networks with Cyclic Symmetries Exhibiting Multiple Clusters
Electronic Supplement

Michael M. Norton,[1,*] Nathan Tompkins,[1,2,*] Baptiste Blanc,[1]
Matthew Carl Cambria,[1] Jesse Held,[1] and Seth Fraden[1,†]

[1] *Physics Department, Brandeis University, Waltham, Massachusetts 02453*
[2] *Physics Department, Wabash University, Crawfordsville, Indiana 47933*

I. MOVIES

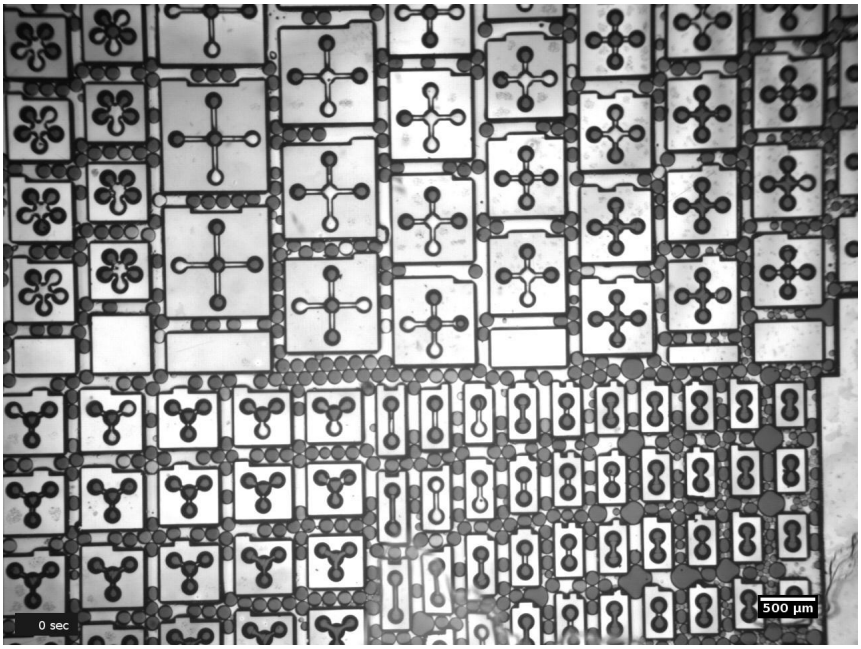

- Movie S1: Reflection microscopy image of an array of networks etched in silicon, loaded with the Belousov-Zhabotinsky emulsion and sealed on top with a glass slide. Bright flashes correspond to the oxidized state of the catalyst.

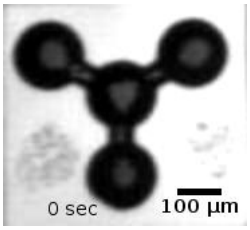

- Movie S2: Phase locking dynamics in a $k = 3$ network with 40 μm separation. Arm nodes oxidize nearly in-phase and at a well defined phase relative to the hub node. The network is imaged using reflected light microscopy, bright flashes correspond to the oxidized state of the catalyst.

* authors contributed equally to this work
† fraden@brandeis.edu

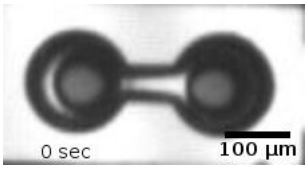

- Movie S3: Phase locking in a $k = 1$ network with 60 μm separation. The pair oscillates with anti-phase synchrony. The network is imaged using reflected light microscopy, bright flashes correspond to the oxidized state of the catalyst.

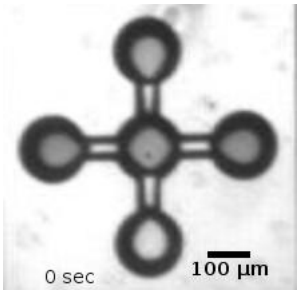

- Movie S4: Phase locking in a $k = 4$ network 60 μm separation. Arm nodes oxidize nearly in-phase and at a well defined phase relative to the hub node. The network is imaged using reflected light microscopy, bright flashes correspond to the oxidized state of the catalyst.

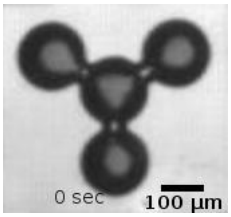

- Movie S5: Unlocked dynamics in a $k = 3$ with 20 μm separation. All nodes oscillate regularly but do not achieve a steady state locking angle (note at $\sim$ 3,400 sec the hub node and lower arm node switch the order in which they oxidize, indicating that they have "slipped" by one another). The network is imaged using reflected light microscopy, bright flashes correspond to the oxidized state of the catalyst.

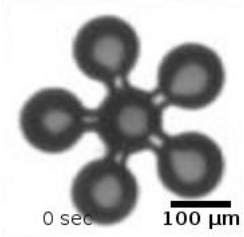

- Movie S6: Center silent dynamics of a $k = 5$ network with 30 μm separation exhibiting center-silent dynamics. Arm-nodes oscillate regularly while the hub node only oxidizes intermittently as a result of the collective inhibition from arm nodes. The network is imaged using reflected light microscopy, bright flashes correspond to the oxidized state of the catalyst.

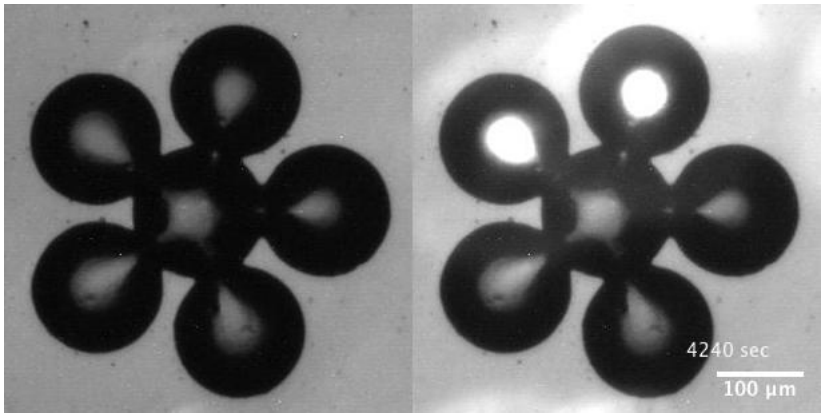

- Movie S7: Center Silent to Locked transition. Reflection microscopy image of a $k = 5$ network with $\sim$1 μm separation. The system begins in the center-silent state: arm-nodes oscillate regularly while the hub node only oxidizes intermittently as a result of the collective inhibition from arm nodes. At $t = 3990$ s blue light (shown in the right panel) is applied to two of the arm nodes, inhibiting their oscillations. The hub node network experiences less inhibition from arm nodes in the now $k = 3$ network and begins oscillating regularly. See Fig. S2 for a space-time plot of the dynamics.

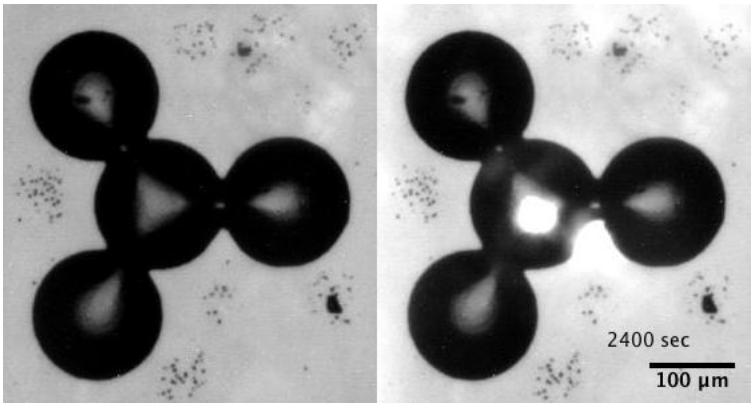

- Movie S8: Perturbation: Locked to Unlocked. Reflection microscopy image of a $k = 3$ network with $\sim$ 1 μm separation. The system begins in the locked state: arm-nodes are nearly synchronized and oscillate at a regular phase-difference with respect to the hub node. At $t = 1990$ s blue light (shown in the right panel) is applied to the hub node, inhibiting its oscillations. Without the hub node to influence the arm nodes, small differences their intrinsic frequencies cause them to slowly de-synchronize. See Fig. S2 for a space-time plot of the dynamics.

II. EXPERIMENTAL METHODS

A. Chemistry

In all experiments 80 mM sulfuric acid, 400 mM malonic acid, 300 mM sodium bromate, 10 mM sodium bromide, and 3 mM ferroin were used. For experiments with illumination 1.2 mM rubpy was added, Fig. S2. These concentrations are summarized in Table SI. The BZ emulsion is created via a flow-focusing microfluidic device with RAN 008 fluorosurfactant and 3M Novec 7500 fluorinated oil, collected in an Eppendorf tube, and pipetted onto the device [1]. Droplets were confined to silicon wells that were $\sim$150 μm in diameter and $\sim$80 μm in depth, Fig. S1.

To prevent characterization based on initial transients the system was given time to stabilize before data was collected and data collection was stopped before the advent of gas bubbles. Gas bubble formation in BZ is inevitable as the breakdown of the organic substrate results in the formation of CO_2 and is a longstanding problem in BZ type reactions [2]. Incompressibility of the fluid and rigidity of the microfluidic cell containing the emulsion prevent bubble formation in our experiments [1]. Over time the seal can be compromised allowing bubbles to form and is an ongoing hurdle in experiments.

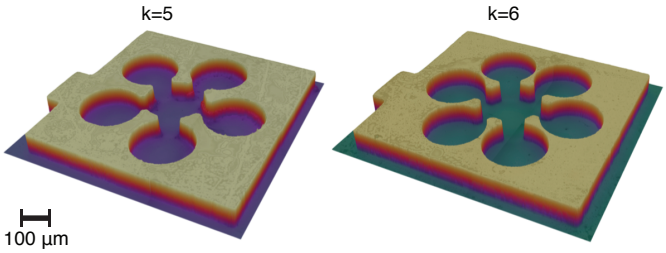

FIG. S1. 3D reconstruction of etched silicon wells for two different star degrees (5 and 6 arms) created using an optical profiler.

Reagent	Formula	Concentration
Sulfuric Acid	H_2SO_4	0.08 M
Malonic Acid	$CH_2(COOH)_2$	0.4 M
Sodium Bromate	$NaBrO_3$	0.3 M
Sodium Bromide	NaBr	0.010 M
Ferroin	$[Fe(o\text{-phen})_3]SO_4$	3 mM
*Rubpy	$[Ru(bpy)_3]Cl_2$	1.2 mM

TABLE SI. Experimental reagent concentrations. *Rubpy was only included for experiments that used optical perturbations, Fig. S2 and movies S7 & S8.

B. Light Perturbations

Although we manufactured star networks in silicon wafers with a fixed topology, we also explored the state diagram by dynamically changing topology using photo-inhibitable chemistry in conjunction with a programmable illumination source [1, 3, 4]. Blue light interacts with the ruthenium catalyst: low levels increase the period of oscillation while high levels result in a stationary chemical state. We used a programmable illumination source to selectively inhibit specific BZ oscillators in a manner analogous to how light is used in opto-genetics to silence individual neurons [4–6]. Shining enough light on a BZ drop to suppress oscillations "prunes" it from the network and effectively transforms that drop into a constant chemical boundary condition.

We induced two different transitions. In the first, a $k = 5$ network is "pruned" to $k = 3$ by optically silencing two outer drops, (Fig. S2a, movie S7). The hub intermittently oscillates when all five outer drops are active. However, the center drop begins oscillating regularly after two of the five arm nodes are silenced ($t \sim 3$ ks) and eventually phase-locks with the remaining three outer drops ($t \sim 9$ ks). In the second, the arm nodes of a $k = 3$ star graph are isolated from each other by optically converting the central drop to a constant-chemical state (Fig. S2b, movie S8). After the application of light, the center (red) drop stops oscillating and the outer three drops transition from synchronous oscillations to phase-slipping, thus demonstrating that the topology has been changed from a connected network of four nodes to three independent oscillators. In both transitions, point model predictions compare well to the observed dynamics.

III. MODELING DETAILS

A. Vanag-Epstein Model of Belousov-Zhabotinsky Reaction

We modeled the Belousov-Zhabotinsky (BZ) reaction using the four-species Vanag-Epstein (VE) model [7]. This model tracks the dynamics of the activator $HBrO_2$ (variable x), inhibitor Br^- (y), oxidized catalyst (z), and the

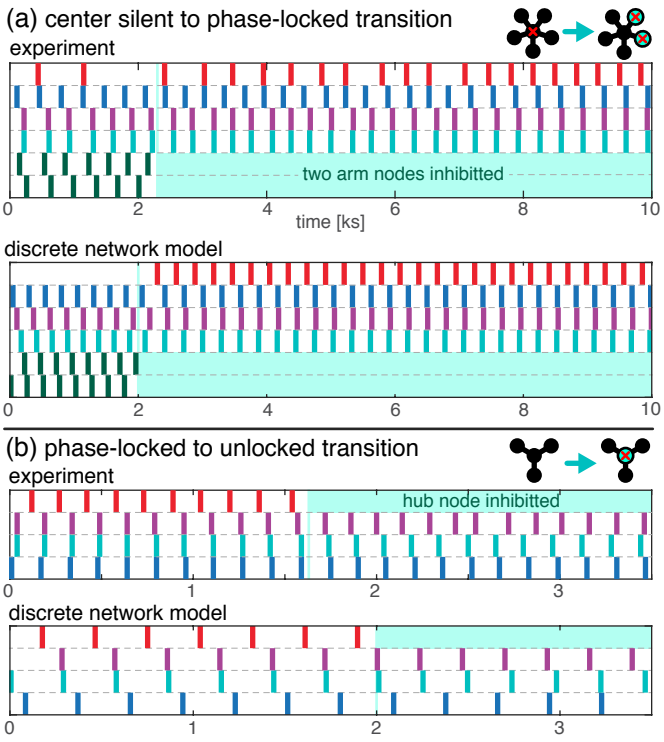

FIG. S2. **On-the-fly topology change.** Space-time plot, each row is an oscillator (hub node is always red) with lines indicating peak in oxidation from data and simulation demonstrating light-induced transitions from the (a) "center-silent" to "locked" and (b) "locked" to "unlocked" states. In (a) two arm nodes are "pruned" from the network, restoring regular hub node oscillations and in (b) the hub node is removed causing arm node de-coherence. Light blue track indicates application of light.

communicator of inhibition Br_2 (u) according to the following rate equations:

$$\begin{aligned} F^x(\mathbf{c}) &= -k_1xy + k_2y - 2k_3x^2 + k_4\frac{x(c_0-z)}{(c_0-z+c_{min})}, \\ F^y(\mathbf{c}) &= -3k_1xy - 2k_2y - k_3x^2 + k_7u + k_9z + k_I\frac{(c_0-z)}{b_c/b+1}, \\ F^z(\mathbf{c}) &= 2k_4\frac{x(c_0-z)}{(c_0-z+c_{min})} - k_9z - k_{10}z + k_I\frac{(c_0-z)}{b_c/b+1}, \\ F^u(\mathbf{c}) &= 2k_1xy + k_2y + k_3x^2 - k_7u, \end{aligned} \tag{S1}$$

where the rate constants are k_1=2×10^6, k_2=$2h^2A$, k_3=3000, k_4=$42ha$, k_7=$29m$, k_{10}=$0.05m$, k_r=2×10^8, k_{red}=5×10^6, and c_{min}=$\sqrt{2k_rc_0(k_9+k_{10})/k_{red}^2}$. The value of k_9 depends on m such that k_9=$0.12m$ for $m > 0.1$ and k_9=$0.07m$ for $m \leq 0.1$. The parameters used for simulations in this work are listed in Table SII. Values for the Malonic acid m, Sodium Bromate a, and Hydrogen h concentrations are chosen according to their experimental values, Table SI. For simulations with light sensitivity, z is the total oxidized catalyst concentration; we do not differentiate between Rubpy and Ferroin.

B. Coupling Strength

To estimate the strength of diffusive coupling μ_{ij}^m of the m^{th} chemical species between BZ drops of radius R, separated by a distance b we idealize the channel connecting drops as a cylinder having radius h and utilize the Derjaguin approximation to find the total molar flux J (mol s^{-1})

$$J_{ij}^m = fD^mP^m\left(c_j^m - c_i^m\right)\mathcal{Y}, \tag{S2}$$

Parameter	Description	Value	Unit
k	Star Degree	1-7	–
R	Drop Diameter	50×10^{-6}	m
b	Oil Gap	1-70$\times10^{-6}$	m
h	Channel Radius	20×10^{-6}	m
D	Diffusion Constant	10^{-9}	$m^2\ s^{-1}$
P_u	Partition Coefficient	2.5	–
f	Fitting (fudge) Factor	0.15	–
a	Bromate	0.3	M
m	Malonic Acid	0.4	M
h_0	Mean Hydrogen	0.16	M
c_0	Total Catalyst (light control)	3 (4.2)	mM
σ_h	Variation in Hydrogen	7.5	%
k_I	Light Inhibition Reaction	1×10^{-6}	$M\ s^{-1}$

TABLE SII. Simulation parameters used in Vanag Epstein-based point model (Eqn. 1 in the main text) and in construction of the phase model.

with diffusivity D and partition coefficient P. These last two parameters, D and P, are not known for bromine in fluorinated oil so we introduce a coupling strength fitting (or fudge) factor f to adjust our estimate. The geometric factor

$$\mathcal{Y} = \int_0^{2\pi} d\theta \int_0^h \frac{\rho d\rho}{\beta\left(\rho\right)}. \tag{S3}$$

with $\beta = 2R - 2\sqrt{R^2-\rho^2} + b$. Integrating gives

$$\mathcal{Y} = \frac{\pi}{2}\left[2\left(\sqrt{R^2-h^2} - R\right) + (b+2R)\ln\left(\frac{b+2R-2\sqrt{R^2-h^2}}{b}\right)\right]. \tag{S4}$$

J_{ij}^m gives the total rate of change of moles for the droplet. To find the rate of change of the concentration, we divide by the volume of the spherical drop. Collecting all terms multiplying the concentration difference yields the expression (with units s^{-1}) for the coupling strength used in the point model (Eqn. 1 in the main text)

$$\mu_{ij}^m = f\frac{D^m P^m \mathcal{Y}}{\frac{4}{3}R^3\pi}. \tag{S5}$$

The limiting case of perfectly planar surfaces can be reached by taking the limit $h/R \to 0$, $\mathcal{Y} \to \pi h^2/b$. In this case

$$\underset{h/R\to 0}{\mu_{ij}^m} = f\frac{D^m P^m}{\frac{4}{3}R^3\pi}\frac{\pi h^2}{b} = f D^m P^m \frac{A}{Vb}. \tag{S6}$$

V is the volume of receiving drop i and A is the cross-sectional area connecting drops i and j.

C. Sensitivity of phase diagram to adjustable parameters

In the main text we introduce both parameter heterogeneity (in the form of varying sulfuric acid concentration) and a factor f to reduce the coupling coefficient from the theoretically value predicted by Eqn. S5. We briefly show the impact of changing these values on the location of the phase boundaries presented in the main text, Fig. S4.

A distribution in intrinsic frequencies results in imperfect synchrony of the arm nodes, Fig. 1 in the main text. Consequently, the hub node receives bromine at multiple times. The sensitivity of the phase diagram on heterogeneity suggests that multiple, small bromine pulses that are spread out in time induce a larger phase delay to the center node than than a single, large pulse. We see evidence for this again when examining the locking angle dependence on k, Fig. 4 in the main text. Without heterogeneity (circles) phase locking persists to large volume ratios. In contrast, heterogeneity (squares), for similar coupling strengths, causes the locking angle trend to more closely follow that of much higher coupling strengths. We leave a detailed investigation of the heterogeneity-dependent locked to center-silent transition to a future work.

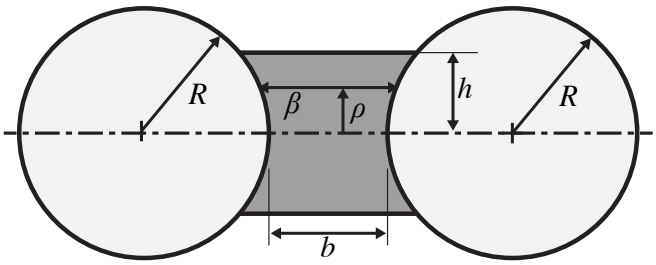

FIG. S3. Schematic used in the calculation of the coupling coefficient, Eqn. S5. For simplicity, the calculation assumes radial symmetry.

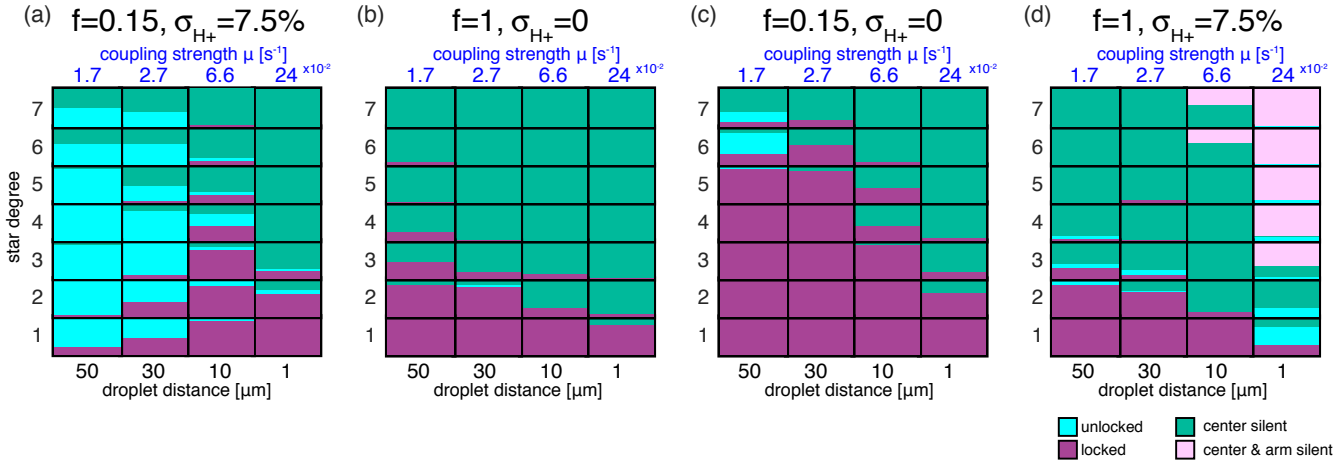

FIG. S4. State diagrams for different tuning parameters. Coupling strength reduction factor f and H^+ concentration variation σ_{H^+} were varied: **(a)** duplicate of phase diagram in main text (Fig. 3) for comparison f=0.15, σ_{H^+}=7.5% **(b)** f=1 σ_{H^+}=0, **(c)** f=0.15, σ_{H^+}=0% **(d)** f=1 σ_{H^+}=7.5%

D. Phase Model

To simplify the fixed point analysis of our system, we employ the method of phase-reduction. Phase-reduction assumes that oscillators interact weakly and only change their phase relative to one-another on a time scale that is longer than a period of oscillation. By coarsening sub-period dynamics only the relative phase between oscillators, rather than their absolute values, is examined [8–10]. Under this prescription, the dynamics of the phase-deviation of the i^{th} oscillator from a free running oscillator in a network has the form

$$\dot{\Phi}_i = \sum\nolimits_{j=1}^{N} \mathcal{A}_{ij} \mathscr{H}_{ij} \left(\Phi_j - \Phi_i\right). \tag{S7}$$

The interaction function $\mathscr{H}_{ij}$ is the period-averaged influence of the i^{th} oscillator from chemical exchange with j^{th} oscillator defined below as

$$\mathscr{H}_{ij} \left(\Phi_j - \Phi_i\right) = \frac{1}{2\pi} \int_0^{2\pi} \mathbf{Q}\left(\theta\right) \cdot \mathbf{M}_{ij} \left(\mathbf{c}_j \left(\theta + \Phi_j - \Phi_i\right) - \mathbf{c}_i \left(\theta\right)\right) d\theta, \tag{S8}$$

where as before $\mathbf{c} = \{x, y, z, u\}$, $\mathbf{M}_{ij}$ is diagonal matrix populated by species-dependent coupling coefficients defined by Eqn. S5. In our case, only the communicator of inhibition u (molecular Bromine) diffuses and we have

$$\mathbf{M}_{ij} = \begin{pmatrix} 0 & 0 & 0 & 0 \\ 0 & 0 & 0 & 0 \\ 0 & 0 & 0 & 0 \\ 0 & 0 & 0 & \mu_{ij}^{u} \end{pmatrix}. \tag{S9}$$

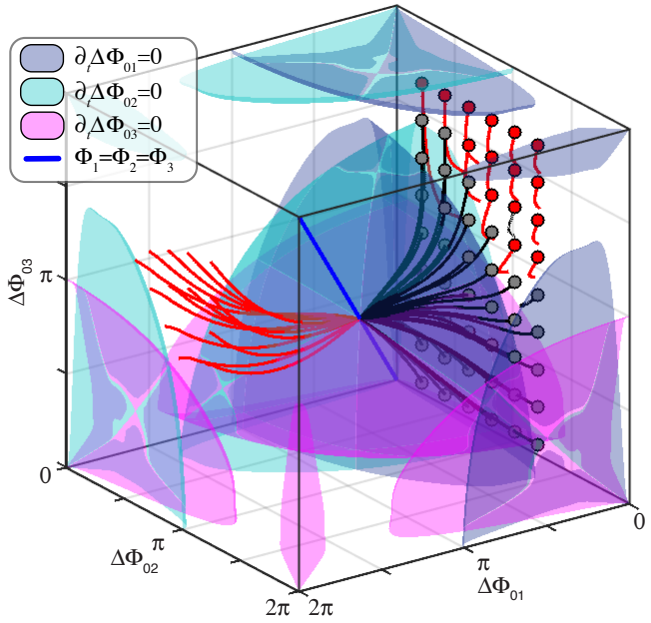

FIG. S5. Phase portrait of a $k = 3$ network with null surfaces (transparent colors) and system trajectories for a coarse selection of initial conditions. Trajectories that proceed directly to the fixed point are labelled in black. Since the dynamics take place on a 3-torus, some initial conditions wrap around the domain before proceeding to the fixed point (red). For a network of identical oscillators, the fixed points lie on the arm-synchronized manifold (blue line).

Q is the phase response curve (PRC) that describes the sensitivity of the oscillator's phase to the addition (or subtraction) of a chemical species. **Q** has units of phase per unit of concentration ($\mathscr{H}_{ij}$ therefore has units of phase per time) and the same dimension as the number of chemical variables (four in the case of the V.E. model). We find **Q** using Malkin's adjoint method [9, 11].

Fig. S5 shows trajectories and null-surfaces for a three-arm ($k = 3$) network. The only fixed points resides along the arm-synchronized manifold (blue line in Fig. S5). If we consider only dynamics along that line $\Phi_a \equiv \Phi_1 = \Phi_2 = \cdots = \Phi_k$ then Eqn. S7 reduces to

$$\begin{aligned} \dot{\Phi}_a &= \mathscr{H}_{a0}\left(\Phi_0 - \Phi_a\right), \\ \dot{\Phi}_0 &= k\mathscr{H}_{0a}\left(\Phi_a - \Phi_0\right). \end{aligned} \tag{S10}$$

Since $\mathscr{H}$ depends only on the relative phase, the dynamics can be written in terms of a single phase difference with no loss in generality $\Phi_{0a} \equiv \Phi_0 - \Phi_a$. The dynamics of the quotient graph

$$\dot{\Phi}_{0a} = k\mathscr{H}_{0a}\left(-\Phi_{0a}\right) - \mathscr{H}_{a0}\left(\Phi_{0a}\right). \tag{S11}$$

are shown in the phase portrait in the main text, Fig. 3.

E. Perturbation Expansion for Locking Angle

To find the leading order dependence of locking angle Φ^*_{0a} on star degree, we begin with the expression for the roots of Eqn. S11.

$$0 = k\mathscr{H}\left(-\Phi^*\right) - \mathscr{H}\left(\Phi^*\right). \tag{S12}$$

To avoid the clutter of subscripts we let $\Phi = \Phi_{0a}$ and so long as we take care to note arguments of the interaction functions, we can also let $\mathscr{H} = \mathscr{H}_{0a} = \mathscr{H}_{a0}$. We then make a change of parameters $\gamma = \log(k)$ and expand the locking angle in a power series $\Phi^* \sim \Phi^{*(0)} + \gamma\Phi^{*(1)} + \gamma^2\Phi^{*(2)} + \mathscr{O}\left(\gamma^3\right)$.

$$0 = e^{\gamma}\mathscr{H}\left(-\left(\Phi^{*(0)} + \gamma\Phi^{*(1)} + \cdots\right)\right) - \mathscr{H}\left(\left(\Phi^{*(0)} + \gamma\Phi^{*(1)} + \cdots\right)\right) \tag{S13}$$

Performing a Taylor expansion about $\gamma = 0$ yields a series of algebraic equations that must be satisfied at each order of γ:

$$\begin{aligned}
\mathscr{O}(1): 0 &= \mathscr{H}\left(-\Phi^{*(0)}\right) - \mathscr{H}\left(\Phi^{*(0)}\right) \\
&\Rightarrow \Phi^{*(0)} = \pi \\
\mathscr{O}(\gamma): 0 &= \mathscr{H}\left(\Phi^{*(0)}\right) - \Phi^{*(1)}\left(\left.\frac{d\mathscr{H}}{d\Phi}\right|_{\Phi^{*(0)}} + \left.\frac{d\mathscr{H}}{d\Phi}\right|_{-\Phi^{*(0)}}\right) \\
&\Rightarrow \Phi^{*(1)} = \frac{1}{2}\mathscr{H}(\Phi)\left(\frac{d\mathscr{H}}{d\Phi}\right)^{-1}\Bigg|_{\Phi=\pi} \\
\mathscr{O}\left(\gamma^2\right): 0 &= \mathscr{H}\left(-\Phi^{*(0)}\right) + \Phi^{*(1)}\left(-2\left.\frac{d\mathscr{H}}{d\Phi}\right|_{-\Phi^{*(0)}} + \left(\left.\frac{d^2\mathscr{H}}{d\Phi^2}\right|_{-\Phi^{*(0)}} - \left.\frac{d^2\mathscr{H}}{d\Phi^2}\right|_{\Phi^{*(0)}}\right)\right) \\
&\quad - 2\Phi^{*(2)}\left(\left.\frac{d\mathscr{H}}{d\Phi}\right|_{\Phi^{*(0)}} + \left.\frac{d\mathscr{H}}{d\Phi}\right|_{-\Phi^{*(0)}}\right) \\
&\Rightarrow \Phi^{*(2)} = 0
\end{aligned} \tag{S14}$$

The solution to the $\mathscr{O}(1)$ problem has multiple solutions; for two identically coupled oscillators $\Phi = 0$ and π are always solutions, though there may be others. Since we are interested in the behavior of the dominant anti-phase attractor $\Phi^* = \pi$, we choose this as our expansion point. Consequently, the coefficients found in Eqn. S14 simplify because $\pi \equiv -\pi \pmod{2\pi}$. Solving for the coefficients $\Phi^{*(\gamma^n)}$ and assembling yields Eqn. 3 from the main text, repeated here:

$$\Phi^* = \pi + \log(k)\frac{1}{2}\mathscr{H}(\Phi)\left(\frac{d\mathscr{H}}{d\Phi}\right)^{-1}\Bigg|_{\Phi=\pi} + \mathscr{O}\left(\gamma^3\right). \tag{S15}$$

We note that because $\mathscr{H}$ and its derivatives are linearly proportional to the coupling strength μ, the final expression for the attractor location is μ-independent.

[1] N. Tompkins, M. C. Cambria, A. L. Wang, M. Heymann, and S. Fraden, *Creation and perturbation of planar networks of chemical oscillators,* Chaos: An Interdisciplinary Journal of Nonlinear Science **25**, 064611 (2015).

[2] O. Qi, W. Y. Tam, P. DeKepper, W. D. McCormick, Z. Noszticzius, and H. L. Swinney, *Bubble-free Belousov-Zhabotinskii-type reactions,* Journal of Physical Chemistry **91**, 2181 (1987).

[3] N. Tompkins, N. Li, C. Girabawe, M. Heymann, G. B. Ermentrout, I. R. Epstein, and S. Fraden, *Testing Turing's theory of morphogenesis in chemical cells.* Proceedings of the National Academy of Sciences of the United States of America **111**, 4397 (2014).

[4] N. Tompkins and S. Fraden, *An inexpensive programmable illumination microscope with active feedback,* American Journal of Physics **84**, 150 (2016).

[5] J. N. Stirman, M. M. Crane, S. J. Husson, S. Wabnig, C. Schultheis, A. Gottschalk, and H. Lu, *Real-time multimodal optical control of neurons and muscles in freely behaving Caenorhabditis elegans.* Nature methods **8**, 153 (2011).

[6] R. Toth and A. F. Taylor, *The tris(2,2'-bipyridyl)ruthenium-catalysed Belousov–Zhabotinsky reaction,* Progress in Reaction Kinetics and Mechanism **31**, 59 (2006).

[7] V. K. Vanag and I. R. Epstein, *A model for jumping and bubble waves in the Belousov-Zhabotinsky-aerosol OT system,* Journal of Chemical Physics **131**, 104512 (2009).

[8] F. C. Hoppensteadt and E. M. Izhikevich, *Weakly Connected Neural Networks*, Applied Mathematical Sciences, Vol. 126 (Springer New York, New York, NY, 1997).

[9] E. M. Izhikevich, *Dynamical Systems in Neuroscience: The Geometry of Excitability and Bursting*, 1st ed. (MIT Press Cambridge, MA, 2007).

[10] T. Stankovski, T. Pereira, P. V. McClintock, and A. Stefanovska, *Coupling functions: Universal insights into dynamical interaction mechanisms,* Reviews of Modern Physics **89**, 045001 (2017).

[11] B. Monga, D. Wilson, T. Matchen, and J. Moehlis, *Phase reduction and phase-based optimal control for biological systems: a tutorial,* Biological Cybernetics **113**, 11 (2019).